THE JOURNAL OF PHYSICAL CHEMISTRY B

Article

pubs.acs.org/JPCB

Photon-by-Photon Hidden Markov Model Analysis for Microsecond Single-Molecule FRET Kinetics

Menahem Pirchi,[†,§] Roman Tsukanov,[‡,§] Rashid Khamis,[†] Toma E. Tomov,[‡] Yaron Berger,[‡] Dinesh C. Khara,[‡] Hadas Volkov,[‡] Gilad Haran,[*,†] and Eyal Nir[*,‡]

[†]Department of Chemical Physics, Weizmann Institute of Science, Rehovot 76100, Israel

[‡]Department of Chemistry and the Ilse Katz Institute for Nanoscale Science and Technology, Ben-Gurion University of the Negev, Beer Sheva 84105, Israel

Supporting Information

ABSTRACT: The function of biological macromolecules involves large-scale conformational dynamics spanning multiple time scales, from microseconds to seconds. Such conformational motions, which may involve whole domains or subunits of a protein, play a key role in allosteric regulation. There is an urgent need for experimental methods to probe the fastest of these motions. Single-molecule fluorescence experiments can in principle be used for observing such dynamics, but there is a lack of analysis methods that can extract the maximum amount of information from the data, down to the microsecond time scale. To address this issue, we introduce H^{2}MM, a maximum likelihood estimation algorithm for photon-by-photon analysis of single-molecule fluorescence resonance energy transfer (FRET) experiments. H^{2}MM is based on analytical estimators for model parameters, derived using the Baum−Welch algorithm. An efficient and effective method for the calculation of these estimators is introduced. H^{2}MM is shown to accurately retrieve the reaction times from ∼1 s to ∼10 μs and even faster when applied to simulations of freely diffusing molecules. We further apply this algorithm to single-molecule FRET data collected from Holliday junction molecules and show that at low magnesium concentrations their kinetics are as fast as ∼10^4 s^{-1}. The new algorithm is particularly suitable for experiments on freely diffusing individual molecules and is readily incorporated into existing analysis packages. It paves the way for the broad application of single-molecule fluorescence to study ultrafast functional dynamics of biomolecules.

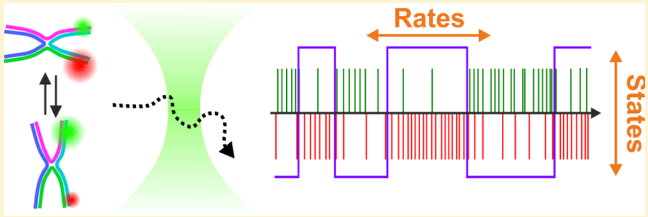

INTRODUCTION

Large-scale conformational changes, often induced by the binding of a substrate or a ligand, are essential for the activity of biomacromolecules, be they proteins or nucleic acids.[1−3] Such conformational transitions may cover a broad range of time scales, from microseconds to seconds. There is a dearth of methods to study dynamics of biomolecules down to microseconds. Thus, popular NMR methods such as relaxation-dispersion spectroscopy[4] cannot obtain rates much faster than 10^3−10^4 s^{-1}. Fluorescence correlation techniques can reach events on the microsecond time scale (and even faster[4,5]) but are limited in their ability to evaluate complex kinetic schemes. Furthermore, correlation methods, like ultrarapid mixing methods,[6] can provide only sums of (forward and backward) kinetic rates, and additional knowledge (i.e., equilibrium propensities of all species) is required to calculate individual rates.

Single-molecule spectroscopy has dramatically changed the way we look at dynamical processes in biophysics and chemistry.[7,8] Using a range of optical methods derived from fluorescence spectroscopy[9] and even Raman spectroscopy,[10] as well as a variety of techniques based on force microscopy,[11] it is now possible to dissect the time courses of reactive processes (e.g., ref 12) and conformational dynamics (e.g., refs 13 and 14) on the level of the individual molecule, thereby overcoming difficulties due to spatial and temporal heterogeneities. Single-molecule fluorescence experiments based on fluorescence resonance energy transfer (FRET)[15] can in principle directly probe the conformational states of a biomolecule at each moment in time and can therefore directly measure separate forward and backward rates, rather than their sums, and characterize multistate kinetics.[16]

Single-molecule FRET experiments can be performed on molecules freely diffusing in solution or immobilized next to a surface. To probe conformational transitions on the microsecond time scale, it is necessary to conduct measurements under conditions that generate a large photon flux.[17] This is more readily achieved with freely diffusing molecules. As their dwell time within the probing laser beam is short, photobleaching at high laser powers is less of a concern. Furthermore, as the molecules passively diffuse through the laser beam, thousands of data sets can be readily obtained in a short time. An additional advantage of experiments on freely diffusing

Received: October 24, 2016
Revised: November 30, 2016
Published: November 30, 2016

DOI: 10.1021/acs.jpcb.6b10726
J. Phys. Chem. B 2016, 120, 13065−13075

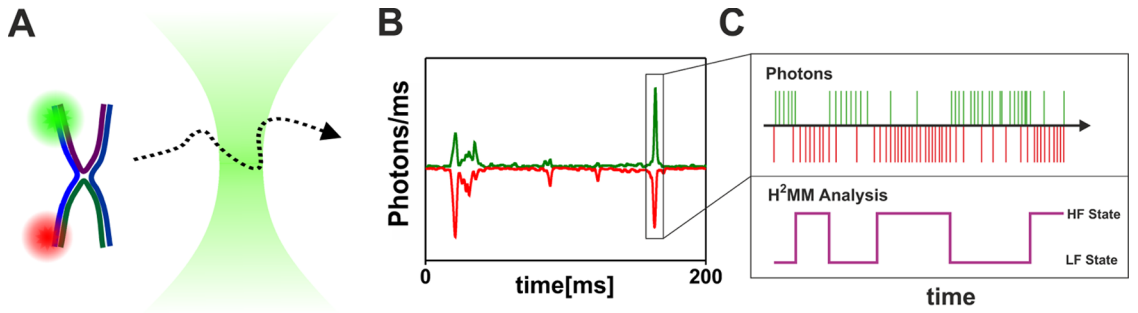

Figure 1. FRET experiments on freely diffusing single molecules reveal transitions between molecular states. When a FRET-labeled molecule diffuses through a focused laser beam (A), it emits a burst of photons in both the donor and acceptor channels (B). H^2MM, a hidden Markov model (HMM) algorithm for photon-by-photon analysis, uses the photon arrival times (marked by green or red lines) and assigns the sequence of conformational states visited by a molecule during a photon burst (C). (HF- high FRET efficiency, LF- low FRET efficiency).

molecules is that the potential influence of the surface on the dynamics does not have to be considered.

A prototypical single-molecule fluorescence experiment involves molecules diffusing in solution and traversing a focused laser beam (Figure 1A). Each time a molecule passes through the beam, it is excited and emits a burst of photons, whose arrival times at the detector are registered. If the molecule is double-labeled for FRET, the photons are split according to color (i.e., donor and acceptor) and registered on two detectors (Figure 1B). Oftentimes the data is used to calculate the average FRET efficiency from each photon burst, and a FRET efficiency histogram is constructed, from which information on the states of the biomolecule is obtained. However, much more information is hidden in the stream of photons, related to transitions between conformational states (Figure 1C).

Our approach for extracting dynamic information from single-molecule photon streams down to the microsecond time scale involves maximum likelihood estimation (MLE)[18] on a photon-by-photon basis. MLE analysis starts with the definition of a particular kinetic model for the experiment. Typically, it is assumed that the kinetic model involves a set of discrete states, whose dynamics are taken as Markovian. The likelihood function for the experimental data, given the kinetic model, is then written, and maximization of this function leads to optimal values for the parameters of the model. As the kinetic states of the studied system are not directly observed in a single-molecule experiment and the observables report only indirectly on these states, the model that describes such a system qualifies as a HMM.[19] In biophysics, HMM techniques have been used for many years to analyze single-ion-channel recordings[20] and have been more recently adapted to analyze single-molecule fluorescence[21−23] and force experiments.[24]

In this article, we introduce H^2MM, a generalized HMM algorithm that uses photon arrival times as input to the analysis, and is particularly suitable for experiments on freely diffusing molecules, where the excitation intensity varies in time. We first provide a detailed description of the algorithm. Then, we demonstrate the capabilities of the method by analysis of synthetic photon-by-photon trajectories generated by simulating the dynamics of freely diffusing molecules. We find that H^2MM operates very well on the simulated trajectories (whose average length is one to several milliseconds). Importantly, the algorithm can retrieve kinetic rates over a very broad range, as fast as 10^5 s^{-1} and as slow as 1 s^{-1} (i.e., much longer than the typical burst duration). Finally, we employ the new algorithm to analyze measurements of molecules of the well-studied Holliday junction (HJ). It has been shown before that HJ dynamics involves two FRET states and that the transition rates between these states increase when the concentration of $MgCl_2$ is lowered.[25−28] We use H^2MM to analyze measurements taken at very low $MgCl_2$ concentrations and show that the rates of interconversion between the states of HJ can be as fast as $\sim 10^4$ s^{-1}.

THEORY

When a double-labeled molecule diffuses through the laser beam, three factors determine the instantaneous number of photons it emits. First, the position of the molecule within the focused laser beam, whose intensity varies in space, determines the molecular excitation rate. This is very different from experiments on immobilized molecules, where the excitation rate is fixed. Second, the emission rate fluctuates due to shot noise. Finally, because of dependency of the energy transfer on the distance between the fluorophores, the conformational state of the molecule changes the relative number of photons emitted from the donor and acceptor. Gopich and Szabo introduced a clever algorithm for the photon-by-photon analysis of single-molecule FRET trajectories,[29] in which the arrival times of the photons are treated as fixed input, whereas the "colors" of the photons (i.e., their origin from donor or acceptor dyes) are assumed to be stochastic variables, dependent on kinetic model parameters. This feature significantly simplifies the analysis, particularly for experiments on freely diffusing molecules, as it allows focusing on the third of the three factors discussed above. Therefore, we adopt it in our algorithm. However, we take a different approach than that by Gopich and Szabo. We write the likelihood function in a way that allows us to adopt the HMM machinery (see eqs 8 and 9 in the Appendix) and, in particular, the Baum−Welch (BW) algorithm.[19] This approach naturally leads to *analytical estimators* for model parameters rather than the numerical solution inherent in other methods.

The BW HMM algorithm has been applied extensively to single-molecule experiments, in which the fluorescence trajectories could be represented in terms of binned quantities (such as fluorescence intensities or FRET efficiencies).[16,21,22] Such trajectories suit very well the standard BW algorithm, which relies on the propagation of the likelihood from one time point to the next. In contrast, a photon-by-photon trajectory contains information only at time points at which a photon was registered. Information is missing between these time points, requiring a generalization of the standard BW algorithm. The missing information can be viewed as another hidden level in

DOI: 10.1021/acs.jpcb.6b10726
J. Phys. Chem. B 2016, 120, 13065−13075

the model, in addition to the indirect relation between observations and kinetic states, and this is why we term the method "H^{2}MM". We show below how to incorporate this second level of missing information into the likelihood and re-derive the expressions for parameter estimators.

H^{2}MM Algorithm. We start with a simplified description of MLE for Markov processes, which allows us to introduce the estimation formulas for H^{2}MM in a compact manner. The full derivation of the H^{2}MM equations is provided in the Appendix.

Consider first a simple Markov process describing memoryless dynamics that involves stochastic transitions among N_s states. We further assume that multiple (experimental or simulated) realizations of this process, termed "Markov chains", are available. One then needs to estimate the optimal parameters that describe the Markov process on the basis of these realizations. Each Markov chain can be described as a time series $X \equiv [x_1, x_2, ..., x_T]$, where x_t is the state of the chain at time t and T is its total length. The initial state probability, that is, the probability that the state of the system at the first time point is i, is defined as $\pi_i \equiv p(x_1 = i)$ and the probability of transition from state i to state j, which is independent of time, is written as $p(x_{t+1} = j|x_t = i) \equiv (\hat{A})_{i,j} = a_{i,j}$. These parameters fully define the model. Given a set of Markov chains, the parameters can be estimated using the MLE approach. The parameter estimators can be written in terms of $\xi(i, j, t) \equiv P(x_t = i, x_{t+1} = j|X, \hat{\lambda})$, which is the probability that chain X has made a transition from i to j at time t, given a particular set of parameters $\hat{\lambda} \equiv [\hat{A}, \vec{\Pi}]$. First, we write an estimator for the transition rates

$$\langle a_{i,j} \rangle = \frac{\sum_{t=1}^{T-1} \xi(i, j, t)}{\sum_{k=1}^{N_s} \sum_{t=1}^{T-1} \xi(i, k, t)} \tag{1}$$

In the case of the analysis of multiple trajectories, an additional sum has to be included and is omitted here and in the following estimators (eqs 2 and 3) for simplicity. In the current simple case, the transitions can be directly observed in trajectory X. Therefore, this expression merely counts the number of transitions from i to j, normalized by the number of opportunities to see these transitions (i.e., the number of times i is visited). By the same token, the estimator for the state probabilities is

$$\langle \pi_i \rangle = \frac{\sum_{k=1}^{N_s} \xi(i, k, 1)}{\sum_{m=1}^{N_s} \sum_{k=1}^{N_s} \xi(m, k, 1)} \tag{2}$$

which equals the number of observed transitions from i to any state during the first time point.

More often than not, the Markov chain is not directly registered but is rather observed through a set of noisy measurements, $Y \equiv [y_1, y_2, ..., y_T]$. In this case, the variant of the above algorithm that optimizes the parameters of a model given the set of measurements is called a HMM. The full specification of a HMM requires augmenting the simple Markov model with the observation probability, that is, the probability $b_{i,k} \equiv P(y_t = k|x_t = i)$ to obtain a value k for the measurement y_t when the system is in state i. This definition assumes a discrete set of possible observation values for the measurements, but it can be readily generalized to include a continuous set of values. If $b_{i,k}$ provides a unique mapping from y_t to x_t, we find ourselves back in the case described above, but when this mapping is not unique, the likelihood function has to take into account all possible state sequences that are commensurate with the sequence of measurements. Thus, although the estimators are still given by eqs 1 and 2 above, the calculation of $\xi(i, j, t)$ is more demanding. This is where the BW algorithm comes to help, providing an ingeniously simple solution in terms of the so-called forward and backward variables (see the Appendix).

Once provided with the means to calculate $\xi(i, j, t)$, we can again use eqs 1 and 2 to obtain estimators for the model parameters, together with eq 3, which provides estimators for $b_{i,k}$

$$\langle b_{i,k} \rangle = \frac{\sum_{t=1}^{T} \sum_{j=1}^{N_s} \xi(i, j, t) \delta_{y_t,k}}{\sum_{t=1}^{T} \sum_{j=1}^{N_s} \xi(i, j, t)} \tag{3}$$

$\langle b_{i,k} \rangle$ is the expected number of times the system is in state i, showing a value k for the measurement.

As $\xi(i, j, t)$ is a function of the model parameters of the current iteration, the calculation of parameter estimators is done iteratively. That is, at each iteration, a new set of estimators is calculated based on the previous set of estimators and the data. A nice property of this algorithm is that it guarantees that the likelihood is increased from one iteration to the next till convergence.[19]

In the above algorithm, each time step involves a transition from one state, i, to another state, j (which could be equal to i). This implies that information about the system exists at each time step. This scenario is relevant, for example, to an intensity-binned single-molecule fluorescence experiment, where each time bin contains a value for the fluorescence intensity or FRET efficiency. A photon-by-photon trajectory differs significantly from this scenario. The arrival of each photon on one of the detectors provides information about the state of the system. However, photons are sparse in time, and it is unknown how the state of the system evolves at time intervals between them. In principle, the system can undergo multiple interstate transitions at unknown times between two consecutive photons. This complication needs to be taken into account in the calculation of the estimators. It is due to this extra layer of missing/hidden information that we call our photon-by-photon algorithm H^{2}MM.

In the framework of H^{2}MM, we start by defining a time unit, short enough so that the probability to find more than one photon within it is negligible (we typically use 1 ns). The time interval between adjacent observed photons can be written as an integer number of time units, that is, $\Delta_{t_n} \equiv t_{n+1} - t_n \in N$. A transition from state i to state j may occur at an arbitrary time, t, between two photon arrival times, that is, $t_n \leq t < t_{n+1}$. Therefore, we generalize $\xi(i, j, t)$ and write it in the following manner

$$\xi(i, j, t) = \sum_{k=1}^{N_s} \sum_{m=1}^{N_s} [P(x_{t_n} = k, x_{t_{n+1}} = m|Y, \hat{\lambda}) \\ P(x_t = i, x_{t+1} = j|x_{t_n} = k, t_{n+1} = m, \hat{\lambda})] \tag{4}$$

The first factor in the brackets is the probability that the states of the system at t_n and t_{n+1} are k and m, respectively, given the observation set Y and model $\hat{\lambda}$. The second factor is the probability that a transition from state i to state j occurred at time t, given that the state of the system upon arrival of the photon preceding t is k and the state of the system upon arrival of the photon following t is m.

At first glance, it might seem that the calculation of $\xi(i, j, t)$ introduces an intensive computational cost, as it needs to be

DOI: 10.1021/acs.jpcb.6b10726
J. Phys. Chem. B 2016, 120, 13065−13075

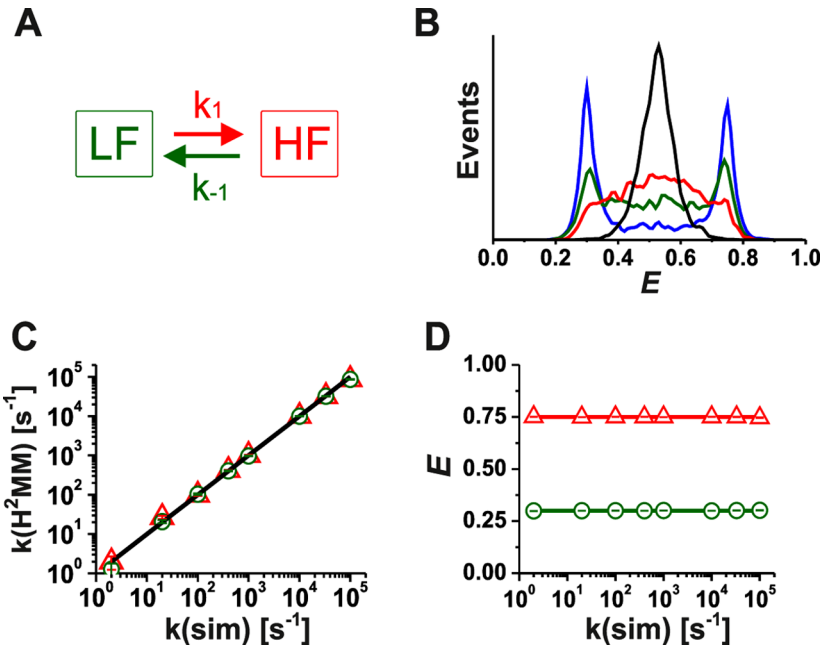

Figure 2. H^2MM analysis of simulated freely diffusing two-state molecules. (A) Schematic of the simulated two-state system with LF and HF states and k_1, k_{-1} transition rates. (B) FRET histograms of the simulated molecules. The results obtained with transition rates 100, 400, 1000, and 10 000 s^{-1} (blue, green, red, and black lines, respectively) are shown. The forward and backward rates were identical ($k_1 = k_{-1}$). (C) Comparison of the simulated transition rates (black line) and the transition rates obtained by H^2MM analysis (k_1, red triangles; k_{-1}, green circles). (D) Comparison of the FRET efficiencies of the simulated HF and LF states (red and green lines, respectively) and those obtained by H^2MM analysis (red triangles and green circles, respectively). Standard errors calculated from several independent simulations are smaller than the symbol sizes.

computed for a large number of time steps between adjacent photons (e.g., for all t, $t_n \leq t < t_{n+1}$). However, we note that the second factor in eq 4, which deals with system evolution between photons, does not depend on the experimental data. Rather, it is a function only of the transition probabilities (see eq 20 in the Appendix). Therefore, we prepare in advance a look-out table that accumulates the values for this factor as a function of the interphoton interval size (Δ_{t_n}). This dramatically accelerates the calculation and makes it scale with the number of photons rather with the number of time units (see the Appendix for details).

The two probability factors in the sum of eq 4 can thus be efficiently calculated by an extension of the HMM-related forward−backward procedure, as detailed in the Appendix. The values of $\xi(i, j, t)$ obtained in this manner can be plugged into estimator eqs 1−3. These equations allow us to obtain optimal parameters from a set of photon-by-photon trajectories given an arbitrary kinetic model adopted for the data. The ensuing algorithm, H^2MM, is a natural extension of the more common HMM algorithm. Familiar software packages or Matlab toolboxes can be readily amended and used to perform this analysis. The Matlab code for H^2MM estimators, based on a freely distributed HMM MATLAB toolkit (http://www.cs.ubc.ca/~murphyk/Software/HMM/hmm.html), is attached as Supporting Information.

RESULTS

H^2MM Analysis of Simulated Data. To test our approach, we applied H^2MM analysis to a set of photon-by-photon single-molecule trajectories generated using numeric simulations of freely diffusing molecules (for details, see the Supporting Information). Each molecule was assumed to interconvert between two states (with low and high FRET efficiency values, called LF and HF, respectively) with rates that we call "forward and backward transition rates" (k_1, k_{-1}, Figure 2A). The FRET efficiency values of the two states were set to match those of HJ molecules (see the next section; LF = 0.30 and HF = 0.75; Figure 2B,D), and the transition rates were varied from k_1, k_{-1} = 10^0−10^5 s^{-1} (dwell times of 1000−0.01 ms, respectively; Figure 2C). The simulated molecules were assumed to emit photons in the donor and acceptor channels as they diffused through a laser spot and generate "fluorescent bursts". The diffusion rate and fluorophore brightness were set such that the burst duration and burst size distributions matched those obtained in the experiments with HJ molecules described below (Figure S1). The simulated data was analyzed using procedures described in the Supporting Information.

FRET histograms obtained from the simulated data are shown in Figure 2B. Double-peaked histograms are obtained when the dynamics is slower than the averaged burst duration, whereas a single-peaked histogram is obtained when the dynamics are faster than the burst duration.[30] Excellent agreement was found between the simulated and H^2MM-retrieved transition rates and FRET efficiencies (Figure 2C,D), indicating that the H^2MM analysis was able to recover the four parameters of the simulated two-state system over the full range of rates examined. The H^2MM analysis results deviated from the simulation by less than 0.1% for the FRET efficiencies for all data points and by less than 9% for all rates excluding the very slow rates (2 s^{-1}). Importantly, even when the simulated rates were significantly slower than the average burst duration (as in the cases with rates of 2 and 20 s^{-1}), H^2MM was still able to retrieve parameters that agreed well with the simulated ones. The excellent agreement between the fitted and simulated parameters was also maintained when the rates were as high as 10^5 s^{-1} (1.3% error). Given the average photon flux in the simulated fluorescence bursts, which rarely exceeded 1000

DOI: 10.1021/acs.jpcb.6b10726
J. Phys. Chem. B 2016, 120, 13065−13075

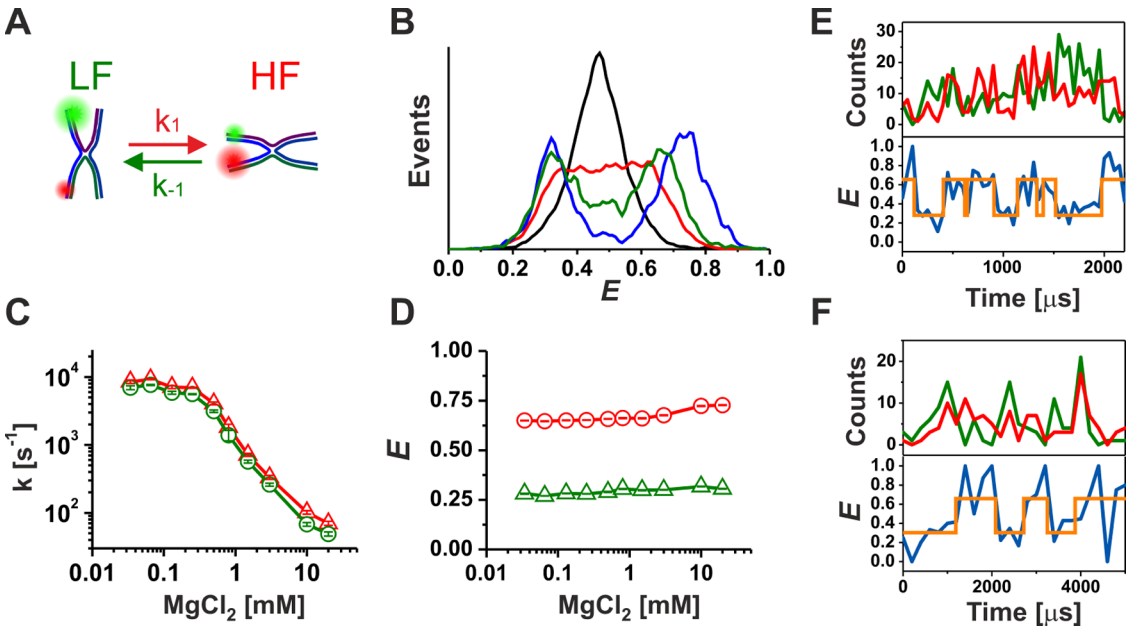

Figure 3. H^2MM analysis of HJ dynamics. (A) Schematic of HJ dynamics with LF and HF states and forward and backward transition rates (k_1 and k_{-1}, respectively). (B) Experimental FRET histograms for HJs measured at 0.034, 1.5, 3.0, and 20 mM $MgCl_2$ concentrations (black, red, green, and blue lines, respectively). (C) H^2MM-retrieved transition rates (k_1 and k_{-1} are shown in red triangles and green circles, respectively). (D) H^2MM-retrieved FRET efficiencies (LF and HF are shown in green triangles and red circles, respectively). The excitation laser power was 100 μW. Error bars are standard deviations calculated from independent experiments measured under identical conditions. (E) Sample single-molecule trajectory obtained from a single photon burst measured at 0.5 mM $MgCl_2$. Upper panel: binned raw data (green, donor; red, acceptor). Lower panel: FRET efficiency calculated from the data (blue), with state annotations from the H^2MM analysis (orange). (F) Sample single-molecule trajectory obtained from a single photon burst measured at 0.8 mM $MgCl_2$. Upper panel: binned raw data (green, donor; red, acceptor). Lower panel: FRET efficiency calculated from the data (blue), with state annotations from the H^2MM analysis (orange).

photons/ms, this finding suggests that even a few photons from each state were sufficient for H^2MM to identify states and transitions between them. This highly attractive feature of the H^2MM algorithm is further discussed below.

Single-Molecule FRET Measurements of HJ Dynamics. To test H^2MM against experimental data, we turned to HJ dynamics (Figure 3A).[25−28] We measured donor- and acceptor-labeled HJ molecules using diffusion-based single-molecule FRET spectroscopy with alternating laser excitation.[30] (For details, see the Supporting Information text and Figure S2.) The experiments were performed over a range of $MgCl_2$ concentrations (0.065−20 mM) that were expected to result in rates spanning over 2−3 orders of magnitudes.[25−28] The first indication of the broad range of rates was a significant dependence of the shapes of the FRET histograms on $MgCl_2$ concentration (Figure 3B). To analyze the data, we applied H^2MM with a two-state model. The optimized transition rates (k_1, k_{-1}) and LF and HF FRET efficiency values are shown in Figure 3C,D, respectively.

The HJ transition rates increased over more than 2 orders of magnitude as the concentration of $MgCl_2$ was decreased (from $\sim 5 \times 10^1$ to $\sim 8 \times 10^3$ s^{-1}). The forward and backward rates were almost identical as is expected for the DNA sequences used in this work. We observed a weak dependence of the FRET efficiencies of the HJ states on the $MgCl_2$ concentration (Figure 3D), which could be a result of minute changes of the HJ conformation or a result of weak influence of $MgCl_2$ on the photophysical properties of the dyes.

Two sample single-molecule trajectories obtained from photon bursts are shown in Figure 3E,F. Photon-by-photon data were binned to present them in the figure. Anticorrelated transitions between the two states on a sub-millisecond time scale are clearly observed in the data. However, intensity variations due to the passage of the molecules through the focused laser beam, as well as photon shot noise, preclude direct state assignment from the trajectories. The H^2MM analysis provides a simple route to state assignment through the Viterbi algorithm (see the Supporting Information), as shown in the figure. It is important to note that the assignment is effectively based on the whole data set, rather than the specific photon burst.

Evaluating the Influence of Acceptor Photophysics. Photophysical processes of the dyes may interfere with the correct retrieval of parameters in the analysis of single-molecule fluorescence data. To examine a possible influence of acceptor blinking on the observed transition rates, we measured HJ molecules using a laser power 3 times stronger than that shown in Figure 2 (300 μW). A stronger laser power may result in increased blinking of both donor and acceptor dyes, but the former would have no influence on the H^2MM analysis,[31] whereas the latter may result in apparently faster transition rates. We analyzed both data measured at low and the high laser power (Figure 4) using a three-state H^2MM model. This model assumed that three states were connected in a row-like fashion with transitions between neighboring states, that is, $S_1 \rightleftarrows S_2 \rightleftarrows S_3$, with S_1 being the low-FRET state, S_2, the high-FRET state, and S_3, a blinking (dark) state. The forward and backward transition rates, the blinking and recovery rates, and the LF-, HF-, and dark-state FRET values are presented in Figure S3.

In the case of low-laser-power measurements, the two- and three-state H^2MM analyses yielded almost identical transition rates (Figure 3), indicating that acceptor blinking did not significantly increase the obtained rates at this laser power. In the case of the high laser power, however, the two-state H^2MM

DOI: 10.1021/acs.jpcb.6b10726
J. Phys. Chem. B 2016, 120, 13065−13075

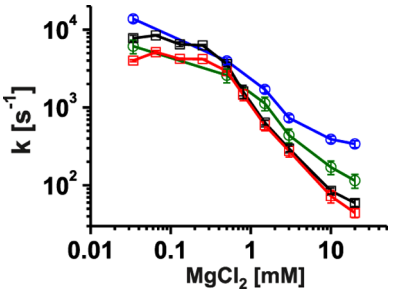

Figure 4. Influence of acceptor blinking on H²MM-retreived transition rates of HJ molecules. Measurements were conducted using low and high laser powers (100 and 300 μW, respectively), and data was analyzed using H²MM with two or three states. Black and red squares: two- and three-state analysis (respectively) of low-laser-power data. Blue and olive circles: two- and three-state analysis (respectively) of high-laser-power data. For clarity, only the averages of forward and backward rates ($(k_1 + k_{-1})/2$) are shown. Error bars are standard deviations calculated from independent experiments measured under identical conditions.

analysis yielded notably faster dynamics (specifically in the high $MgCl_2$ concentration regime where the transition rates are slow), and a three-state H²MM analysis mitigated some of the blinking effect on the extracted rates. Transitions between the LF and the dark state, ignored in the above description, are in principle also possible. Accordingly, we analyzed the HJ data using a four-state H²MM model, where both the LF and HF states had a corresponding dark state. In some cases, the analysis yielded almost identical transition rates to the above, and in other cases, the analysis yielded results that pointed to the problems in convergence of this rather complex model (data not shown). Therefore, we limit detailed analysis to two- and three-state models.

Considering these results, we conclude that acceptor blinking may slightly influence the retrieved transition rates; however, using different laser power and a H²MM model that considers explicitly a dark state, it should be possible to asses and mitigate the influence of blinking.

Comparison of H²MM and Probability Distribution Analysis (PDA). To further test the validity of the parameters obtained with the new method, we also analyzed our data using the PDA (see the Supporting Information text)[30] and compared the results to those of H²MM (Figure S4). The PDA method extracts transition rates and FRET efficiency values by fitting the FRET distributions. This approach effectively bins the data according to burst durations (1−5 ms). As a result, the PDA could not reliably resolve dynamics faster than ∼3 ms (see the Supporting Information text and Figure S4). The PDA transition rates were slower by about 50% than those obtained with the two-state H²MM. Analysis of simulated data showed that PDA underestimates the transition rates by about 20−30% (Figure S5), whereas no systematic errors were observed in H²MM analysis of simulated data (Figure 2).

DISCUSSION

In this work, we introduced a novel algorithm for photon-by-photon analysis of single-molecule FRET data, H²MM. The new method is especially geared towards experiments on freely diffusing molecules and fully utilizes the advantages of the HMM analysis machinery, including the BW algorithm and related methods. In these two aspects, it deviates significantly from previous work that used numerical methods to maximize a photon-by-photon likelihood[29,32−34] or from the work that focused on immobilized molecules, where the average fluorescence intensity could be assumed constant.[35] Using HMM analysis allows us to obtain analytical expressions for parameter estimators, which can be readily incorporated into existing HMM packages. The latter feature is a major advantage, as it facilitates the implementation of the method by nonexpert practitioners. Furthermore, relying on analytical expressions, rather than numerical analysis, implies more robust optimization procedures. Indeed, it has been shown that the BW algorithm guarantees that the likelihood never decreases from one iteration of the analysis to the next.[19] In addition, the use of analytical expressions for estimators facilitates generalization of the analysis to an arbitrary number of states.[36] This capability may be useful for the analysis of complex folding scenarios or complex conformational dynamics and further enables treatment of photophysical artifacts, as shown above.

Through analysis of simulated data, we showed that H²MM accurately retrieves transition statistics over 5 orders of magnitude of time. First, because the analysis is done on a photon-by-photon basis, the full time resolution provided by the measured flux of photons is utilized. Thus, with a photon flux of 10^6 photons/s, which is high yet not very difficult to achieve in experiments on diffusing molecules, one can readily retrieve transition times of a few microseconds. Interestingly, with such fast switching times between states, the FRET histogram would typically show a single peak (the fast exchange limit). Therefore, FRET histogram-based methods such as PDA may fail to obtain the correct transition rates, whereas H²MM has no such problem. Second, because the analysis takes into account the whole statistics obtained from multiple fluorescence bursts, including bursts that do not show any transitions between states, it is possible to obtain state-to-state transition times that are significantly longer than burst durations. This is because transition times that are X times slower than the diffusion time of the molecules through the laser beam will still be found in $1/X$ of the bursts. The sensitivity to slow dynamics could be further improved if recurrences of the same molecule through the beam are taken into account. Hoffmann et al.[37] showed that the probability that two consecutive bursts originate from the same molecule can be calculated directly from the data and taken into account. We intend to integrate this capability into the H²MM analysis, thereby improving the sensitivity of the method to slow dynamics even further.

To demonstrate the significant utility of H²MM, we applied it here to analyze experimental data on HJ molecules at the limit of very fast dynamics, that is, essentially in the absence of magnesium. We were able to identify rates that are 5−10 times faster than those reported previously.[25,27] We argue that H²MM should be useful for a broad spectrum of problems in fast dynamics of biomolecules. For example, we envision that H²MM will facilitate the study of domain closure in enzymes or binding-induced conformational transitions, processes that may occur on the microsecond time scale. Obviously, the ability to recover fast dynamics depends on the photon flux and the FRET efficiency difference between states (as well as other parameters). Nevertheless, the introduction of the H²MM algorithm provides a clear route for the application of single-molecule fluorescence spectroscopy on freely diffusing molecules for studying fast dynamics.

DOI: 10.1021/acs.jpcb.6b10726
J. Phys. Chem. B 2016, 120, 13065−13075

APPENDIX: THE H²MM ALGORITHM

In this appendix, we describe in detail the theory behind H²MM while drawing on its relation to standard HMM methodology, specifically the BW algorithm and the related forward−backward procedure.

Let Y be a sequence of M observations, $Y \equiv [y_1, y_2, ..., y_M]$, which represent the color of photons detected from a single molecule at times $\vec{T} \equiv [t_1, t_2, ..., t_M]$, where $\vec{T}$ is given in terms of our defined time unit, τ (see below). The color representation of photons is discretized, that is, $y_t \in [1, 2, ..., N_p]$, where N_p is the number of symbols used to represent photon color categories. In the single-molecule FRET experiment, photons are usually classified into two categories, so that $y_t \in [1,2]$, where "1"/"2" represent "green"/"red" photons, respectively.

Note that the photons are detected at random; hence, the time interval between adjacent observations is not constant but is nevertheless an integer number, that is

$$\Delta_{t_n} \equiv t_{n+1} - t_n \in N$$

To achieve the maximum possible temporal resolution, we choose τ such that $\tau \ll \text{mean}(\Delta_{t_n})$. In this work, τ is 1 ns.

The evolution of the state of a molecule is described by a Markov chain, with N_s states. The Markov chain is denoted $X \equiv [x_1, x_2, ..., x_{t_M}]$, where x_t is the state at time t, that is, $x_t \in [1, 2, ..., N_s]$. The complete HMM used to analyze the data is denoted here $\hat{\lambda}$ and has three types of parameters:

First, $\vec{\Pi}$ is the initial probability vector of the states of the molecule, such that $(\vec{\Pi})_i$ is the probability that state i is populated in the first time point

$$(\vec{\Pi})_i \equiv \pi_i = P(x_1 = i|\hat{\lambda}) \tag{5}$$

where $1 \le i \le N_s$.

Second, $\hat{A}$ is the transition probability matrix, that is, $(\hat{A})_{i,j}$ is the probability of transition from state i to state j; this quantity is independent of time, as required for a time-homogeneous Markov chain

$$(\hat{A})_{i,j} \equiv a_{i,j} = P(x_{t+1} = j|x_t = i, \hat{\lambda}) \text{ for all } t \text{ and } 1 \le i, j \le N_s \tag{6}$$

Finally, $\hat{B}$ is the emission probability matrix, that is, $(\hat{B})_{i,k}$ is the probability of observing symbol k in state i.

$$(\hat{B})_{i,k} \equiv b_{i,k} = P(y_t = k|x_t = i, \hat{\lambda}), \text{ for all } t \text{ and } \begin{Bmatrix} 1 \le i \le N_s \\ 1 \le k \le N_p \end{Bmatrix} \tag{7}$$

where N_p is the total number of different observation symbols. It is worth noting that $\vec{\Pi}$, $\hat{A}$, and $\hat{B}$ are row stochastic, that is, $\begin{Bmatrix} \sum_{k=1}^{N_s} \pi_k = 1 \\ \sum_{k=1}^{N_s} a_{i,k} = 1,\ 1 \le i \le N_s \\ \sum_{k=1}^{N_s} b_{i,k} = 1 \end{Bmatrix}$, and are also independent of each other.

The likelihood function, $L(Y, \hat{\lambda})$, is defined as the probability to obtain the observation sequence, Y, as a function of the model parameters

$$L(Y, \hat{\lambda}) \equiv P(Y|\hat{\lambda}) = \sum_X [P(X, Y|\hat{\lambda})] \tag{8}$$

where the sum is carried over all possible realizations of X.

The summand on the right-hand side of eq 8, that is, $P(X, Y|\hat{\lambda})$, is the joint probability of Y and any realization of X, given $\hat{\lambda}$. $P(X, Y|\hat{\lambda})$ is given by

$$P(X, Y|\hat{\lambda}) = P(X|\hat{\lambda})\cdot P(Y|X, \hat{\lambda}) = \pi_{x_{t_1}} \prod_{n=1}^{M-1} [A^{\Delta t_n}_{x_{t_n}, x_{t_{n+1}}}]\cdot \prod_{n=1}^{M} [b_{x_{t_n}, y_{t_n}}] \tag{9}$$

where

$$\begin{Bmatrix} \pi_{x_{t_1}} \equiv P(x_{t_1}|\hat{\lambda}) = \sum_{k=1}^{N_s} [\pi_k \cdot \delta_{x_1,k}], \text{ with } \delta_{i,j} \equiv \begin{cases} 1, & i = j \\ 0, & i \ne j \end{cases} \\ b_{x_{t_n}, y_{t_n}} \equiv P(y_{t_n}|x_{t_n}, \hat{\lambda}) = \sum_{k=1}^{N_s} \sum_{m=1}^{N_p} [\delta_{x_{t_n},k} \cdot b_{k,m} \cdot \delta_{m,y_{t_n}}] \\ A^{\Delta t_n}_{x_{t_n}, x_{t_{n+1}}} = P(x_{t_{n+1}}|x_{t_n}, \hat{\lambda}) = \sum_{k=1}^{N_s} \sum_{m=1}^{N_s} [\delta_{x_{t_n},k} \cdot (\hat{A}^{\Delta t_n})_{k,m} \cdot \delta_{m,x_{t_{n+1}}}] \end{Bmatrix}$$

Note that eq 9 reduces to the familiar HMM expression for $P(X, Y|\hat{\lambda})$[19] if Δt_n is set to 1 for all $n \in [1, 2, ..., M-1]$.

In the Supporting Information, we exploit this similarity to formally show that the HMM parameter re-estimation formulas (eqs 1−3) also apply in the H²MM case. Here, we proceed to derive the algorithm to calculate $\xi(i, j, t)$.

As shown in eq 4 of the main text, $\xi(i, j, t)$ can be written as a sum over two factors

$$\xi(i, j, t) \equiv P(x_t = i, x_{t+1} = j|Y, \hat{\lambda}) = \sum_{k=1}^{N_s} \sum_{m=1}^{N_s} [P(x_{t_n} = k, x_{t_{n+1}} = m|Y, \hat{\lambda}) P(x_t = i, x_{t+1} = j|x_{t_n} = k, t_{n+1} = m, \hat{\lambda})] \tag{4a}$$

DOI: 10.1021/acs.jpcb.6b10726
J. Phys. Chem. B 2016, 120, 13065−13075

where t is assumed to lie within the Δ_{t_n} interval, that is, $t_n \le t < t_{n+1}$.

The first factor of eq 4a is denoted $\xi^*(k, m, t_n) \equiv P(x_{t_n} = k, x_{t_{n+1}} = m|Y, \hat{\lambda})$, and is the likelihood that states k and m were populated at times t_n and t_{n+1}, respectively, given observation sequence Y and parameter set $\hat{\lambda}$. This factor is calculated using a procedure which is a straightforward generalization of the HMM-related forward−backward procedure.

First, a forward variable is defined as $\alpha^*(i, t_n) \equiv P([y_{t_1}, y_{t_2}, ..., y_{t_n}], X_{t_n} = i|\hat{\lambda})$, that is, the probability of the partial observation sequence $[y_{t_1}, y_{t_2}, ..., y_{t_n}]$ (until time t_n) and of state i at time t_n, given $\hat{\lambda}$. α^* is computed using the following recursion rules:

Initialization step

$$\alpha^*(i, t_1) = \pi_i b_{i,y_{t_1}} \tag{10}$$

where $b_{i,y_{t_1}} \equiv \sum_{k=1}^{N_s} b_{i,k}\, \delta_{k,y_{t_1}}$, and forward recursion step

$$\alpha^*(i, t_{n+1}) = \sum_{k=1}^{N_s} \alpha^*(k, t_n) \hat{A}_{k,i}^{\Delta_{t_n}} b_{i,y_{t_{n+1}}} \tag{11}$$

For comparison, the standard HMM counterpart to eq 11 is given by

$$\alpha(i, t_{n+1}) = \sum_{k=1}^{N_s} \alpha(k, t_n) \hat{A}_{k,i}^{1} b_{i,y_{t_{n+1}}} \tag{12}$$

Second, a backward variable is defined as $\beta^*(j, t_n) \equiv P([y_{t_{n+1}}, y_{t_{n+2}}, ..., y_{t_M}]|x_{t_n} = j, \hat{\lambda})$, that is, the likelihood of the partial observation sequence from t_{n+1} to the end, given state j at time t_n and $\hat{\lambda}$. β^* is computed by the following recursion rules:

Initialization step

$$\beta^*(i, t_M) = 1 \tag{13}$$

and backward recursion step

$$\beta^*(i, t_{n-1}) = \sum_{k=1}^{N_s} \hat{A}_{i,k}^{\Delta_{t_{n-1}}} \beta^*(k, t_n) b_{k,y_{t_n}} \tag{14}$$

For standard HMM, we have

$$\beta(i, t_{n-1}) = \sum_{k=1}^{N_s} \hat{A}_{i,k}^{1} \beta(k, t_n) b_{k,y_{t_n}} \tag{15}$$

In practice, and for reasons related to numerical precision, normalized versions of α^* and β^* are used

$$\alpha'(i, t_n) = \frac{\alpha^*(i, t_n)}{c_\alpha(t_n)} \tag{16}$$

$$\beta'(i, t_n) = \frac{\beta^*(i, t_n)}{c_\beta(t_n)} \tag{17}$$

where $c_\alpha(t_n)$ and $c_\beta(t_n)$ are given by $\left\{ \begin{array}{l} c_\alpha(t_n) = \sum_{k=1}^{N_s} \alpha^*(k, t_n) \\ c_\beta(t_n) = \sum_{k=1}^{N_s} \beta^*(k, t_n) \end{array} \right\}$.

The normalization factors can in fact be used to calculate the likelihood through

$$\log L(Y, \lambda) = \sum_{n=1}^{M} \log(c_\alpha(t_n)) = \sum_{n=1}^{M} \log(c_\beta(t_n)) \tag{18}$$

Using α' and β', we can calculate $\xi^*(k, m, t_n)$ as

$$\xi^*(k, m, t_n) = \frac{\alpha'(k, t_n)(A^{\Delta_{t_n}})_{k,m} \beta'(m, t_{n+1}) b_{m,y_{t_{n+1}}}}{\sum_{k'=1}^{N_s} \sum_{m'=1}^{N_s} [\alpha'(k', t_n)(A^{\Delta_{t_n}})_{k',m'} \beta'(m', t_{n+1})] b_{m',y_{t_{n+1}}}} \tag{19}$$

The second factor in eq 4a, $P(x_t = i, x_{t+1} = j|x_{t_n} = k, t_{n+1}\, m, \hat{\lambda})$, is the probability of having a transition from state i to j at time t, $t_n \le t < t_{n+1}$, given that the states at t_n and t_{n+1} are k and m, respectively, and given $\hat{\lambda}$. This factor can be written as follows

$$\begin{aligned} &P(x_t = i, x_{t+1} = j|x_{t_n} = k, x_{t_{n+1}} = m, \hat{\lambda}) \\ &= \frac{P(x_t = i, x_{t+1} = j, x_{t_{n+1}} = m|x_{t_n} = k, \hat{\lambda})}{P(x_{t_{n+1}} = m|x_{t_n} = k, \hat{\lambda})} \\ &= \frac{\hat{A}_{k,i}^{(t-t_n)} \cdot a_{i,j} \cdot \hat{A}_{j,m}^{(t_{n+1}-t-1)}}{\hat{A}^{\Delta_{t_n}}{}_{k,m}} \end{aligned} \tag{20}$$

where $t_n \le t < t_{n+1}$ and $1 \le k, m, i, j \le N_s$.

Using $\xi^*(k, m, t_n)$ of eq 19 and $P(X_t = i, X_{t+1} = j|X_{t_n} = k, X_{t_{n+1}} = m, \hat{\lambda})$ of eq 20, we can now compute $\xi(i, j, t)$ of eq 4a, which can in turn be substituted into the parameter re-estimation equations (eqs 1−3), thus essentially providing an exact solution to the H^{2}MM parameter optimization problem.

However, this is not a tractable solution, as the number of time points for which we need to compute $\xi(i, j, t)$ scales inversely with τ. We show below how one can reduce the computational cost and make the number of computations scale with the number of photons.

To this end, we make the following definition

$$\begin{aligned} \rho_{k,m,i,j}(\Delta_{t_n}) = &\sum_{t=t_n}^{t_{n+1}-1} P(x_t = i, x_{t+1} = j, x_{t_{n+1}} \\ &= m|x_{t_n} = k, \hat{\lambda}) \end{aligned} \tag{21}$$

ρ is a sum over the numerator of the right-hand side of eq 20.

Before deriving an expression for ρ, let us demonstrate its usefulness in reducing the computational cost.

Using eqs 4a, 19, and 21, we can express $\sum_{t=t_n}^{t_{n+1}-1} \xi(i, j, t)$, the expected number of transitions from state i to j during the Δ_{t_n} interval, as

$$\sum_{t=t_n}^{t_{n+1}-1} \xi(i, j, t) = \sum_{k=1}^{N_s} \sum_{m=1}^{N_s} \left[\frac{\xi^*(k, m, t_n) \rho_{k,m,i,j}(\Delta_{t_n})}{\hat{A}^{\Delta_{t_n}}{}_{k,m}} \right] \tag{22}$$

We can substitute this relation into the transition probability re-estimation formula (eq 1) and get

$$\langle a_{i,j} \rangle = \frac{\sum_{n=1}^{M-1} \sum_{k=1}^{N_s} \sum_{m=1}^{N_s} \left[\frac{\xi^*(k, m, t_n) \rho_{k,m,i,j}(\Delta_{t_n})}{\hat{A}^{\Delta_{t_n}}{}_{k,m}} \right]}{\sum_{n=1}^{M-1} \sum_{k=1}^{N_s} \sum_{m=1}^{N_s} \sum_{z=1}^{N_s} \left[\frac{\xi^*(k, m, t_n) \rho_{k,m,i,z}(\Delta_{t_n})}{\hat{A}^{\Delta_{t_n}}{}_{k,m}} \right]} \tag{23}$$

DOI: 10.1021/acs.jpcb.6b10726
J. Phys. Chem. B 2016, 120, 13065−13075

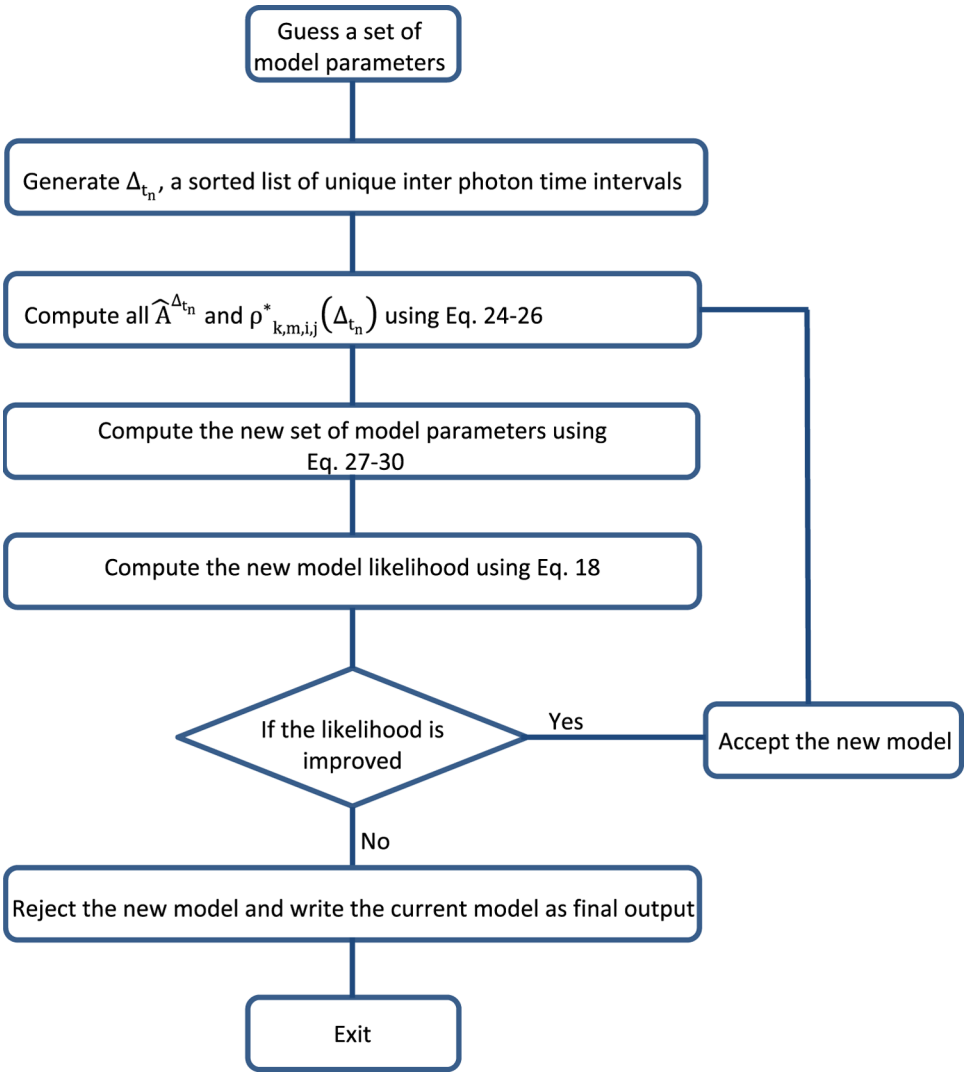

Figure 5. Flowchart of H^{2}MM analysis. The flowchart shows the practical progress of the analysis based on the equations in the Appendix. The Matlab code for H2MM analysis is attached as a Supporting Information.

In this equation, M is the total number of photons.

The estimator of eq 23 requires computation of $\xi^*(k, m, t_n)$ at the photon arrival times and computation of $\rho_{k,m,i,j}(\Delta_{t_n})$ for all unique interphoton intervals Δ_{t_n} in the data. Therefore, the number of steps related to the latter calculation scales with the number of photons rather than the number of time units. To implement this calculation, we need to derive an expression for $\rho_{k,m,i,j}(\Delta_{t_v})$, which is done by forward recursion:

Initialization step

$$\rho_{k,m,i,j}(\Delta_t = 1) = \delta_{k,i} a_{i,j} \delta_{j,m} \tag{24}$$

and recursion step

$$\rho_{k,m,i,j}(\Delta_t + 1) = \sum_{z=1}^{N_s} \rho_{k,z,i,j}(\Delta_t) a_{z,m} + \hat{A}_{k,i}^{\Delta_t} a_{i,j} \delta_{j,m} \tag{25}$$

The first term on the right-hand side of eq 25 corresponds to transitions between states i and j that occur during the interval Δ_t. The second term represents a transition that occurs in the new time interval following Δ_t. Using the recursion rules of eqs 24 and 25, we need to calculate $\rho_{k,m,i,j}(\Delta_t)$ for all unique values of Δ_t in the range $[1, 2, ..., \max(\Delta_{t_n})]$. We can do even fewer calculations if we generalize eq 25 in the following manner:

Generalized recursion step

$$\rho_{k,m,i,j}(\Delta_{t_v} + \Delta_{t_q}) = \sum_{z=1}^{N_s} [\rho_{k,z,i,j}(\Delta_{t_v}) \hat{A}_{z,m}^{\Delta_{t_q}}] + \sum_{z=1}^{N_s} [\hat{A}_{k,z}^{\Delta_{t_v}} \rho_{z,m,i,j}(\Delta_{t_q})] \tag{26}$$

where both Δ_{t_v} and Δ_{t_q} are integers.

To fully utilize the recursion rule of eq 26, we define $\vec{\Delta}_t$, an augmented list of interphoton time intervals. This list is predominantly composed of the unique interphoton intervals in the data. Additional elements in $\vec{\Delta}_t$ are auxiliary intervals selected to guarantee that every interval in $\vec{\Delta}_t$ (apart from $\Delta_t = 1$) can be written as a sum of two smaller intervals, that is, $\Delta_{t_u} = \Delta_{t_v} + \Delta_{t_q}$, where $\Delta_{t_u}, \Delta_{t_v}, \Delta_{t_q} \in \vec{\Delta}_t$. As an example, let us consider the following set of time intervals, [3, 5, 9, 10, 12], to

DOI: 10.1021/acs.jpcb.6b10726
J. Phys. Chem. B 2016, 120, 13065−13075

which we will need to add [1, 2, 4] and thus get $\overrightarrow{\Delta}_t$ = [1, 2, 3, 4, 5, 9, 10, 12], which can be written as [1, 1 + 1, 1 + 2, 1 + 3, 1 + 4, 4 + 5, 1 + 9, 2 + 10].

Now we have in our hands all the ingredients for the estimation of parameters based on the H^{2}MM algorithm. We conclude this Appendix by giving the complete H^{2}MM estimation formulas written for the important case of multiple independent trajectories

$$\langle a_{i,j}\rangle = \frac{\sum_{l=1}^{W}\sum_{n=1}^{M_l-1}\sum_{k=1}^{N_s}\sum_{m=1}^{N_s}\left[\frac{\xi_l^*(k,m,t_n)\rho_{k,m,i,j}(\Delta_{t_n})}{\hat{A}^{\Delta_{t_n}}{}_{k,m}}\right]}{\sum_{l=1}^{W}\sum_{n=1}^{M_l-1}\sum_{k=1}^{N_s}\sum_{m=1}^{N_s}\sum_{z=1}^{N_s}\left[\frac{\xi_l^*(k,m,t_n)\rho_{k,m,i,z}(\Delta_{t_n})}{\hat{A}^{\Delta_{t_n}}{}_{k,m}}\right]} \tag{27}$$

where W is the number of trajectories, M_l is the number of photons in the l'th trajectory, and the subscript l in ξ_l^* denotes that it was evaluated for the l'th trajectory.

$$\langle b_{i,k}\rangle = \frac{\sum_{l=1}^{W}\sum_{n=1}^{M_l}\sum_{j=1}^{N_s}\xi_l(i,j,t_n)\delta_{y_{t_n},k}}{\sum_{l=1}^{W}\sum_{n=1}^{M_l}\sum_{j=1}^{N_s}\xi_l(i,j,t_n)} \tag{28}$$

where $\sum_{k=1}^{N_s}\xi_l(i,k,t_n)$ can be written as

$$\sum_{k=1}^{N_s}\xi_l(i,k,t_n) = \frac{\alpha_l'(i,t_n)\beta_l'(i,t_n)}{\sum_{m=1}^{N_s}[\alpha_l'(m,t_n)\beta_l'(m,t_n)]} \tag{29}$$

and

$$\langle \pi_i\rangle = \frac{\sum_{l=1}^{W}\sum_{k=1}^{N_s}\xi_l(i,k,t_1)}{\sum_{l=1}^{W}\sum_{m=1}^{N_s}\sum_{k=1}^{N_s}\xi_l(m,k,t_1)} \tag{30}$$

The flowchart in Figure 5 shows how to combine all the procedures above into one algorithm that is used to compute the final model estimators.

■ ASSOCIATED CONTENT

Supporting Information

The Supporting Information is available free of charge on the ACS Publications website at DOI: 10.1021/acs.jpcb.6b10726.

Additional experimental results, experimental methods, and additional theoretical methods (PDF)

Matlab code files for H^{2}MM including a user guide and simple simulations that allow the user to test the code (ZIP)

■ AUTHOR INFORMATION

Corresponding Authors

*E-mail: gilad.haran@weizmann.ac.il (G.H.).

*E-mail: eyalnir@bgu.ac.il (E.N.).

ORCID

Gilad Haran: 0000-0003-1837-9779

Author Contributions

§M.P. and R.T. contributed equally to this work.

Notes

The authors declare no competing financial interest.

■ ACKNOWLEDGMENTS

This work is supported by grants from the Israel Science Foundation (1578/13, E.N. and 686/14, G.H.). G.H. thanks the kind support of the Gerhardt M.J. Schmidt Minerva Center of Supramolecular Architecture. We thank Haim Aviram for multiple discussions on this manuscript.

■ REFERENCES

(1) Grant, B. J.; Gorfe, A. A.; McCammon, J. A. Large Conformational Changes in Proteins: Signaling and Other Functions. *Curr. Opin. Struct. Biol.* **2010**, *20*, 142−7.

(2) Changeux, J. P. Allostery and the Monod-Wyman-Changeux Model after 50 Years. *Annu. Rev. Biophys.* **2012**, *41*, 103−33.

(3) Guo, J.; Zhou, H. X. Protein Allostery and Conformational Dynamics. *Chem. Rev.* **2016**, *116*, 6503−15.

(4) Baldwin, A. J.; Kay, L. E. Nmr Spectroscopy Brings Invisible Protein States into Focus. *Nat. Chem. Biol.* **2009**, *5*, 808−14.

(5) Nettels, D.; Gopich, I. V.; Hoffmann, A.; Schuler, B. Ultrafast Dynamics of Protein Collapse from Single-Molecule Photon Statistics. *Proc. Natl. Acad. Sci. U.S.A.* **2007**, *104*, 2655−60.

(6) Lapidus, L. J. Exploring the Top of the Protein Folding Funnel by Experiment. *Curr. Opin. Struct. Biol.* **2013**, *23*, 30−5.

(7) Moerner, W. E. Single-Molecule Spectroscopy, Imaging, and Photocontrol: Foundations for Super-Resolution Microscopy (Nobel Lecture). *Angew. Chem., Int. Ed. Engl.* **2015**, *54*, 8067−93.

(8) Selvin, P. R.; Ha, T. *Single Molecule Techniques: A Laboratory Manual*; Cold Spring Harbor Laboraotory Press, 2007.

(9) Gell, C.; Brockwell, D. J.; Smith, A. *Handbook of Single Molecule Fluorescence Spectroscopy*; Oxford University Press, 2006.

(10) Kneipp, K.; Kneipp, H. Single Molecule Raman Scattering. *Appl. Spectrosc.* **2006**, *60*, 322A−334A.

(11) Bustamante, C. In Singulo Biochemistry: When Less Is More. *Annu. Rev. Biochem.* **2008**, *77*, 45−50.

(12) English, B. P.; Min, W.; van Oijen, A. M.; Lee, K. T.; Luo, G.; Sun, H.; Cherayil, B. J.; Kou, S. C.; Xie, X. S. Ever-Fluctuating Single Enzyme Molecules: Michaelis-Menten Equation Revisited. *Nat. Chem. Biol.* **2006**, *2*, 87−94.

(13) Hanson, J. A.; Duderstadt, K.; Watkins, L. P.; Bhattacharyya, S.; Brokaw, J.; Chu, J. W.; Yang, H. Illuminating the Mechanistic Roles of Enzyme Conformational Dynamics. *Proc. Natl. Acad. Sci. U.S.A.* **2007**, *104*, 18055−18060.

(14) Seo, M. H.; Park, J.; Kim, E.; Hohng, S.; Kim, H. S. Protein Conformational Dynamics Dictate the Binding Affinity for a Ligand. *Nat. Commun.* **2014**, *5*, 3724.

(15) Michalet, X.; Weiss, S.; Jager, M. Single-Molecule Fluorescence Studies of Protein Folding and Conformational Dynamics. *Chem. Rev.* **2006**, *106*, 1785−813.

(16) Pirchi, M.; Ziv, G.; Riven, I.; Cohen, S. S.; Zohar, N.; Barak, Y.; Haran, G. Single-Molecule Fluorescence Spectroscopy Maps the Folding Landscape of a Large Protein. *Nat. Commun.* **2011**, *2*, 493.

(17) Oikawa, H.; Suzuki, Y.; Saito, M.; Kamagata, K.; Arai, M.; Takahashi, S. Microsecond Dynamics of an Unfolded Protein by a Line Confocal Tracking of Single Molecule Fluorescence. *Sci. Rep.* **2013**, *3*, 2151.

(18) Pawitan, Y. *In All Likelihood: Statistical Modelling and Inference Using Likelihood*; Oxford University Press, 2013.

(19) Rabiner, L. R. A Tutorial on Hidden Markov-Models and Selected Applications in Speech Recognition. *Proc. IEEE* **1989**, *77*, 257−286.

(20) Colquhoun, D.; Hawkes, A. G.; Srodzinski, K. Joint Distributions of Apparent Open and Shut Times of Single-Ion Channels and Maximum Likelihood Fitting of Mechanisms. *Philos. Trans. R. Soc. London, Ser. A* **1996**, *354*, 2555−2590.

(21) Andrec, M.; Levy, R. M.; Talaga, D. S. Direct Determination of Kinetic Rates from Single-Molecule Photon Arrival Trajectories Using Hidden Markov Models. *J. Phys. Chem. A* **2003**, *107*, 7454−7464.

(22) McKinney, S. A.; Joo, C.; Ha, T. Analysis of Single-Molecule Fret Trajectories Using Hidden Markov Modeling. *Biophys. J.* **2006**, *91*, 1941−1951.

(23) Bronson, J. E.; Fei, J.; Hofman, J. M.; Gonzalez, R. L., Jr.; Wiggins, C. H. Learning Rates and States from Biophysical Time Series: A Bayesian Approach to Model Selection and Single-Molecule Fret Data. *Biophys. J.* **2009**, *97*, 3196−3205.

(24) Stigler, J.; Ziegler, F.; Gieseke, A.; Gebhardt, J. C.; Rief, M. The Complex Folding Network of Single Calmodulin Molecules. *Science* **2011**, *334*, 512−516.
(25) McKinney, S. A.; Declais, A. C.; Lilley, D. M.; Ha, T. Structural Dynamics of Individual Holliday Junctions. *Nat. Struct. Biol.* **2003**, *10*, 93−97.
(26) Gietl, A.; Holzmeister, P.; Grohmann, D.; Tinnefeld, P. DNA Origami as Biocompatible Surface to Match Single-Molecule and Ensemble Experiments. *Nucleic Acids Res.* **2012**, *40*, No. e110.
(27) Kim, J. Y.; Kim, C.; Lee, N. K. Real-Time Submillisecond Single-Molecule Fret Dynamics of Freely Diffusing Molecules with Liposome Tethering. *Nat. Commun.* **2015**, *6*, No. 6992.
(28) Krainer, G.; Hartmann, A.; Schlierf, M. Farfret: Extending the Range in Single-Molecule Fret Experiments Beyond 10 Nm. *Nano Lett.* **2015**, *15*, 5826−9.
(29) Gopich, I. V.; Szabo, A. Decoding the Pattern of Photon Colors in Single-Molecule Fret. *J. Phys. Chem. B* **2009**, *113*, 10965−10973.
(30) Tsukanov, R.; Tomov, T. E.; Berger, Y.; Liber, M.; Nir, E. Conformational Dynamics of DNA Hairpins at Millisecond Resolution Obtained from Analysis of Single-Molecule Fret Histograms. *J. Phys. Chem. B* **2013**, *117*, 16105−16109.
(31) Kong, X.; Nir, E.; Hamadani, K.; Weiss, S. Photobleaching Pathways in Single-Molecule Fret Experiments. *J. Am. Chem. Soc.* **2007**, *129*, 4643−4654.
(32) Chung, H. S.; McHale, K.; Louis, J. M.; Eaton, W. A. Single-Molecule Fluorescence Experiments Determine Protein Folding Transition Path Times. *Science* **2012**, *335*, 981−984.
(33) Chung, H. S.; Gopich, I. V.; McHale, K.; Cellmer, T.; Louis, J. M.; Eaton, W. A. Extracting Rate Coefficients from Single-Molecule Photon Trajectories and Fret Efficiency Histograms for a Fast-Folding Protein. *J. Phys. Chem. A* **2011**, *115*, 3642−3656.
(34) Ramanathan, R.; Munoz, V. A Method for Extracting the Free Energy Surface and Conformational Dynamics of Fast-Folding Proteins from Single Molecule Photon Trajectories. *J. Phys. Chem. B* **2015**, *119*, 7944−7956.
(35) Okamoto, K.; Sako, Y. Variational Bayes Analysis of a Photon-Based Hidden Markov Model for Single-Molecule Fret Trajectories. *Biophys. J.* **2012**, *103*, 1315−1324.
(36) Khreich, W.; Granger, E.; Miri, A.; Sabourin, R. A Survey of Techniques for Incremental Learning of Hmm Parameters. *Inform. Sci.* **2012**, *197*, 105−130.
(37) Hoffmann, A.; Nettels, D.; Clark, J.; Borgia, A.; Radford, S. E.; Clarke, J.; Schuler, B. Quantifying Heterogeneity and Conformational Dynamics from Single Molecule Fret of Diffusing Molecules: Recurrence Analysis of Single Particles (Rasp). *Phys. Chem. Chem. Phys.* **2011**, *13*, 1857−1871.

■ NOTE ADDED AFTER ASAP PUBLICATION

This paper published ASAP on 12/15/2016. The Supporting Information was amended and the revised version was reposted on 12/29/2016.

DOI: 10.1021/acs.jpcb.6b10726
J. Phys. Chem. B 2016, 120, 13065−13075